in solution and the solid-state ^{13}C spectra were obtained by using a Bruker CXP 200 spectrometer. For all the variable-temperature experiments, a VT-1000 machine was used. Temperatures mentioned in Figures 1–3 are known with an accuracy of ±1 K. The solid-state ^{13}C spectra (CP MAS) were recorded with use of the standard PENMR method, including a rotation frequency of the sample of 3000–4000 Hz. The contact time introduced was 5 ms.

Acknowledgment. We thank Dr. P. Jackson for many helpful discussions and the CNRS and the Academy of Sciences of the USSR for financial support.

Square Fe_2Au_2 and Triangular Fe_2Au Clusters: A Reversible Transformation. X-ray Crystal Structure of $[Fe_2Au_2(CO)_8(\mu\text{-dppm})]$ (dppm = Bis(diphenylphosphino)methane)

Santiago Alvarez,* Oriol Rossell,* Miquel Seco, and Jordi Valls

Departament de Química Inorgànica, Universitat de Barcelona, Diagonal, 647, 08028 Barcelona, Spain

Maria Angela Pellinghelli and Antonio Tiripicchio*

Istituto di Chimica Generale ed Inorganica, Università di Parma, Centro di Studio per la Strutturistica Diffrattometrica del CNR, Viale delle Scienze 78, 43100 Parma, Italy

Received October 22, 1990

The salt $(NEt_4)_2[Fe_2(CO)_8]$ reacts with $(ClAu)_2(\mu\text{-L})$ (L = bis(diphenylphosphino)methane (dppm), 1,2-bis(diphenylphosphino)ethane (dppe), 1,3-bis(diphenylphosphino)propane (dppp)) in tetrahydrofuran to yield $[Fe_2Au_2(CO)_8(\mu\text{-L})]$ (L = dppm, **2a**; L = dppe, **2b**; L = dppp, **2c**). The structure of **2a** has been determined by X-ray diffraction methods. Crystals are monoclinic, space group $P2_1/n$, with $Z = 4$ in a unit cell of dimensions $a = 16.405$ (5) Å, $b = 17.031$ (8) Å, $c = 12.410$ (4) Å and $\beta = 95.64$ (2)°. The structure has been solved from diffractometer data by direct and Fourier methods and refined by full-matrix least squares on the basis of 3640 observed reflections to R and R_w values of 0.0291 and 0.0318, respectively. The metal core consists of an unprecedented, nearly square tetrametallic Fe_2Au_2 framework with Au–Au = 2.915 (1) Å, Au–Fe = 2.527 (2) and 2.534 (2) Å, and Fe–Fe = 2.900 (2) Å distances. **2a** does not react with an excess of $(NEt_4)_2[Fe_2(CO)_8]$, but **2b,c** add another $[Fe_2(CO)_8]^{2-}$ fragment to give the hexametallic complexes $(NEt_4)_2[\{Fe_2Au(CO)_6(\mu\text{-CO})\}_2(\mu\text{-L})]$ (L = dppe, **3b**; L = dppp, **3c**), which are postulated to be formed by two Fe_2Au units joined by an L ligand. Furthermore, **3b,c** react reversibly with 1 equiv of $(ClAu)_2(\mu\text{-L})$ to again afford **2b,c**, respectively. An extended Hückel molecular orbital study of the bonding capabilities of two forms of $[Fe_2(CO)_8]^{2-}$ has been carried out. Formation of terminal Fe–Au bonds is found to be only compatible with the unbridged form of $[Fe_2(CO)_8]^{2-}$, whereas the formation of a triangular Fe_2Au cluster is most favorable for the bridged form of the iron–carbonyl fragment. Several alternative semibridging interactions between carbonyls and Au atoms in $[Fe_2Au_2(CO)_8(\mu\text{-dppm})]$ are analyzed, and the structure with only one cis-equatorial carbonyl bent toward each Au atom is found to be the most stable one.

Introduction

Numerous studies have concentrated on the synthesis of mixed-metal cluster compounds in which the $AuPR_3$ (R = alkyl, aryl) moiety is incorporated into structures containing other transition metals. At present, derivatives containing two or more $AuPPh_3$ units are the subject of much current interest.[1] This is due in part to the easy occurrence of direct Au–Au bonds in such species that makes the proposed isolobal relationship between a hydride and a $AuPPh_3$ unit[2] not always strictly applicable with respect to the structures adopted by hydrides and gold phosphine substituted transition-metal clusters.[3]

We have recently described the complex $(NEt_4)[Fe_2(CO)_6(\mu\text{-CO})_2(\mu\text{-AuPPh}_3)]$, and its X-ray analysis revealed that the iron–iron bond is bridged by a $AuPPh_3$ fragment, giving a triangular Fe_2Au unit.[4] Now, we wish to report the synthesis of several mixed-metal clusters containing Fe_2Au and Fe_2Au_2 skeletons. Moreover, we describe an unprecedented reaction in solution involving both types of derivatives, $Fe_2Au_2(\mu\text{-L}) + Fe_2 \rightarrow (Fe_2Au)_2(\mu\text{-L})$, and we report the X-ray crystal structure of the compound $[Fe_2Au_2(CO)_8(\mu\text{-dppm})]$ (**2a**; dppm = bis(diphenylphosphino)methane).

Results and Discussion

As described earlier,[4] the reaction of $ClAuPPh_3$ with $(NEt_4)_2[Fe_2(CO)_8]$ in tetrahydrofuran (THF) gives orange-brown microcrystals of the complex $(NEt_4)[Fe_2(CO)_6(\mu\text{-CO})_2(\mu\text{-AuPPh}_3)]$ (1). Remarkably, the addition of an excess of the gold derivative to $(NEt_4)_2[Fe_2(CO)_8]$ solutions did not afford the tetrametallic cluster $[Fe_2Au_2(CO)_8(PPh_3)_2]$, and 1 was recovered unaltered. Steric strains derived from the bulky $AuPPh_3$ fragment were postulated to be responsible for the inertness of 1 in incorporating an additional gold fragment. This argument is supported by the fact that, according to theoretical molecular orbital calculations (see below), the negative charge of the Fe_2Au complex is localized mostly on the sterically crowded Fe atoms. In order to obtain the Fe_2Au_2

(1) Salter, I. D. *Adv. Organomet. Chem.* **1989**, *29*, 249.
(2) Lauher, J. W.; Wald, K. *J. Am. Chem. Soc.* **1981**, *103*, 7648.
(3) (a) Bruce, M. I.; Nicholson, B. K. *J. Organomet. Chem.* **1983**, 252, 243. (b) Bateman, L. W.; Green, M.; Mead, K. A.; Mills, R. M.; Salter, I. D.; Stone, F. G. A.; Woodward, P. *J. Chem. Soc., Dalton Trans.* **1988**, 2599. (c) Bruce, M. I.; Nicholson, B. K. *Organometallics* **1984**, *3*, 101.
(4) Rossell, O.; Seco, M.; Jones, P. J. *Inorg. Chem.* **1990**, *29*, 348.

0276-7333/91/2310-2309$02.50/0

complexes, we modified our initial strategy and we decided to use digold compounds of the type $(ClAu)_2(\mu\text{-L})$ (L = bidentate phosphine), having in mind that the bite angle of such species could favor the simultaneous coordination of both gold atoms to the iron centers in $[Fe_2(CO)_8]^{2-}$. It should be noted that recently Salter has been able to form mixed ruthenium–gold clusters by reacting preformed cluster dianions and $(ClM)_2(\mu\text{-L})$ (M = Cu, Ag, Au).[5] In fact, the salt $(NEt_4)_2[Fe_2(CO)_8]$ reacts in a few minutes with $(AuCl)_2(\mu\text{-dppm})$ in THF in a 1:1 molar ratio at −20 °C to give a red-orange solution, from which $[Fe_2Au_2(CO)_8(\mu\text{-dppm})]$ (**2a**) can be isolated as air-stable red microcrystals. Its ^{31}P NMR spectrum has a singlet at room temperature, and the elemental analysis suggests the proposed formula. Interestingly, the IR spectrum both in solution and as a KBr pellet does not show bands in the bridging carbonyl region, in contrast to those observed for the trimetallic cluster **1**. A reasonable explanation based on molecular orbital calculations will be given below.

The synthetic approach for **2a** was applied to the analogous complexes $[Fe_2Au_2(CO)_8(\mu\text{-L})]$ (L = dppe (**2b**), dppp (**2c**)) in order to study the effect, on the stability and reactivity of these species, of the replacement of the dppm ligand by other diphosphines containing longer chains. It was found that the aerial and thermal stability of such compounds decreases according to **2a** > **2b** > **2c**; the last compound could not be isolated in a pure form because it decomposed in solution at temperatures as low as −20 °C. Steric strains, postulated to follow the inverse sequence **2a** < **2b** < **2c**, may account for the different stabilities of **2a–c**. Thus, an increase of the chain length in L goes along with a lengthening of the iron–iron bond and consequently a decrease in the final stability.

On the other hand, the behavior of complexes **2** in solution in the presence of an excess of the salt $(NEt_4)_2[Fe_2(CO)_8]$ was also investigated. While THF solutions of **2a** remain unaltered after several hours at room temperature, **2b,c** react quantitatively, affording products that show $\nu(CO)$ patterns in the IR spectra practically superimposable with that observed for complex **1**, with bands corresponding to bridging carbonyl ligands. In addition, the resulting products have only one peak in their ^{31}P NMR spectrum, a fact suggesting the formation of complexes with high symmetry. Remarkably, the addition of 1 equiv of $(AuCl)_2(\mu\text{-L})$ to these solutions allows us to reverse the process to **2b** or **2c**, according to IR and ^{31}P NMR spectroscopy. These results can be easily interpreted in terms of the reaction shown in eq 1, which involves the species **2b,c** and the new hexametal compounds **3b,c** containing two Fe_2Au units bridged by a diphosphine ligand.

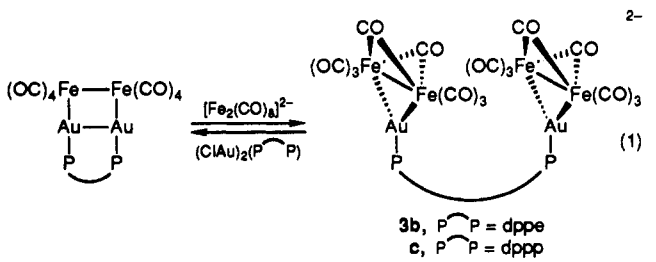

Compound **3b** was characterized by elemental analysis and spectroscopic techniques, but unfortunately we were not able to grow single crystals for an X-ray structure determination. Complex **3c** is less stable than **3b** and could not be isolated as a pure compound. However, its $\nu(CO)$ pattern in the IR spectrum is identical with that shown by **3b**, confirming the proposed structure. Once more, the higher reactivity shown by **2b,c** in comparison to that of **2a** should be related to the steric strain caused by the presence of two and three CH_2 units in the L chain in the former compounds, respectively. To the best of our knowledge, the process described here does not have precedent in the literature and opens an interesting entry into the synthesis of complexes containing two independent metal clusters joined by bridging ligands.

To confirm the structure proposed for **2a**, a single-crystal X-ray structure determination was carried out.

Table I. Selected Bond Distances (Å) and Angles (deg) with Esd's in Parentheses for Compound 2a

Au(1)–Au(2)	2.915 (1)	P(1)–C(9)	1.854 (8)
Au(1)–Fe(1)	2.534 (2)	P(1)–C(10)	1.801 (9)
Au(2)–Fe(2)	2.527 (2)	P(1)–C(16)	1.811 (10)
Fe(1)–Fe(2)	2.900 (2)	P(2)–C(9)	1.834 (8)
Au(1)–P(1)	2.278 (2)	P(2)–C(22)	1.816 (9)
Au(2)–P(2)	2.274 (2)	P(2)–C(28)	1.791 (9)
Fe(1)–C(1)	1.77 (1)	C(1)–O(1)	1.16 (1)
Fe(1)–C(2)	1.75 (1)	C(2)–O(2)	1.16 (1)
Fe(1)–C(3)	1.77 (1)	C(3)–O(3)	1.16 (1)
Fe(1)–C(4)	1.79 (1)	C(4)–O(4)	1.15 (1)
Fe(2)–C(5)	1.78 (1)	C(5)–O(5)	1.14 (1)
Fe(2)–C(6)	1.76 (1)	C(6)–O(6)	1.16 (1)
Fe(2)–C(7)	1.76 (1)	C(7)–O(7)	1.17 (1)
Fe(2)–C(8)	1.76 (1)	C(8)–O(8)	1.13 (1)
Au(2)–Au(1)–Fe(1)	89.18 (5)	C(5)–Fe(2)–C(7)	101.8 (5)
Au(1)–Au(2)–Fe(2)	85.73 (5)	C(5)–Fe(2)–C(8)	97.1 (5)
Au(1)–Fe(1)–Fe(2)	85.93 (6)	C(6)–Fe(2)–C(7)	151.5 (5)
Au(2)–Fe(2)–Fe(1)	89.66 (6)	C(6)–Fe(2)–C(8)	93.0 (5)
Au(2)–Au(1)–P(1)	92.26 (8)	C(7)–Fe(2)–C(8)	92.8 (5)
Fe(1)–Au(1)–P(1)	177.39 (8)	Au(1)–P(1)–C(9)	112.3 (3)
Au(1)–Au(2)–P(2)	90.14 (7)	Au(1)–P(1)–C(10)	115.0 (3)
Fe(2)–Au(2)–P(2)	172.68 (9)	Au(1)–P(1)–C(16)	113.4 (3)
Au(1)–Fe(1)–C(1)	70.3 (3)	C(9)–P(1)–C(10)	103.2 (4)
Au(1)–Fe(1)–C(2)	93.4 (3)	C(9)–P(1)–C(16)	105.4 (4)
Au(1)–Fe(1)–C(4)	79.6 (3)	C(10)–P(1)–C(16)	106.6 (4)
Fe(2)–Fe(1)–C(1)	93.0 (3)	Au(2)–P(2)–C(9)	108.2 (3)
Fe(2)–Fe(1)–C(3)	86.9 (4)	Au(2)–P(2)–C(22)	117.9 (3)
Fe(2)–Fe(1)–C(4)	81.0 (3)	Au(2)–P(2)–C(28)	115.4 (3)
C(1)–Fe(1)–C(2)	91.8 (5)	C(9)–P(2)–C(22)	104.8 (4)
C(1)–Fe(1)–C(3)	102.6 (5)	C(9)–P(2)–C(28)	105.9 (4)
C(1)–Fe(1)–C(4)	149.7 (4)	C(22)–P(2)–C(28)	103.5 (4)
C(2)–Fe(1)–C(3)	94.5 (5)	Fe(1)–C(1)–O(1)	174.0 (8)
C(2)–Fe(1)–C(4)	93.7 (4)	Fe(1)–C(2)–O(2)	177.7 (9)
C(3)–Fe(1)–C(4)	106.7 (5)	Fe(1)–C(3)–O(3)	177.4 (9)
Au(2)–Fe(2)–C(6)	79.3 (4)	Fe(1)–C(4)–O(4)	176.1 (8)
Au(2)–Fe(2)–C(7)	72.9 (3)	Fe(2)–C(5)–O(5)	176.7 (10)
Au(2)–Fe(2)–C(8)	88.8 (3)	Fe(2)–C(6)–O(6)	174.5 (10)
Fe(1)–Fe(2)–C(5)	85.0 (3)	Fe(2)–C(7)–O(7)	174.9 (9)
Fe(1)–Fe(2)–C(6)	80.5 (4)	Fe(2)–C(8)–O(8)	178.1 (9)
Fe(1)–Fe(2)–C(7)	92.9 (3)	P(1)–C(9)–P(2)	113.3 (4)
C(5)–Fe(2)–C(6)	105.2 (5)		

Description of the X-ray Structure of $[Fe_2Au_2(CO)_8(\mu\text{-dppm})]$ (2a). The structure of the cluster **2a** is depicted in Figure 1 together with the atomic numbering scheme; the most important bond distances and angles are given in Table I. The metal core of **2a** consists of an unprecedented tetrametallic Fe_2Au_2 framework. The short Au–Au (2.915 (1) Å), Au–Fe (2.527 (2) and 2.534 (2) Å), and Fe–Fe (2.900 (2) Å) distances suggest a tetrahedrally distorted square geometry with the vertices occupied by the iron and gold atoms. The tetrahedral distortion is shown by the deviations of metal atoms from the mean plane passing through them (Au (1), 0.159 (1) Å; Au(2), −0.160 (1) Å; Fe(1), −0.395 (2) Å; Fe(2), 0.384 (2) Å) and by the dihedral angle between the two Au(1)Au(2)Fe(1) and Au(1)Au(2)Fe(2) triangles (24.7 (1)°). This metal arrangement is rare in the chemistry of gold[6] and has only

(5) Brown, S. S. D.; Salter, I. D.; Dent, A. J.; Kitchen, G. F. M.; Orpen, A. G.; Bates, P. A.; Hursthouse, M. B. *J. Chem. Soc., Dalton Trans.* **1989**, 1227.

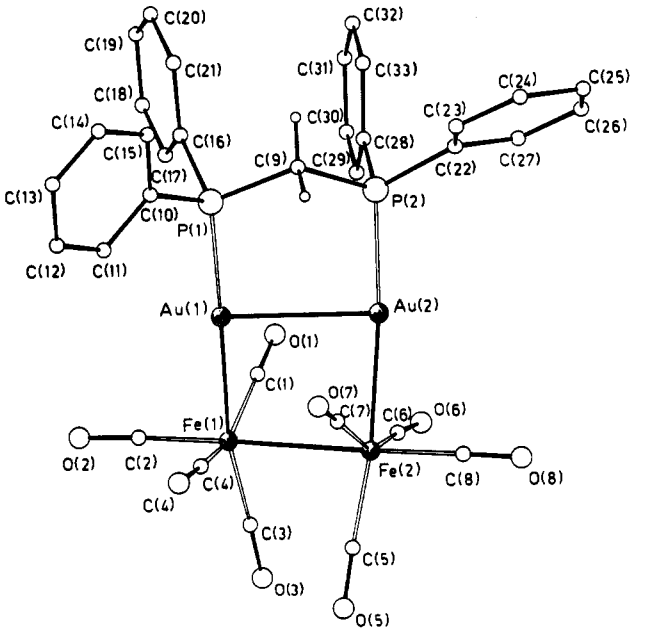

Figure 1. View of the molecular structure of $[Fe_2Au_2(CO)_8(\mu\text{-dppm})]$ (**2a**) with the atomic labeling scheme.

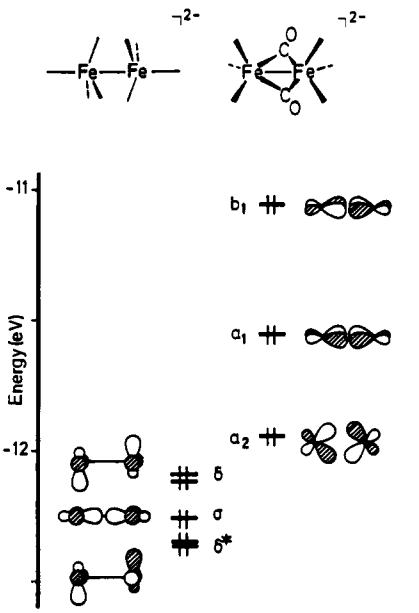

Figure 2. Valence orbitals of the unbridged (left) and bridged (right) forms of $[Fe_2(CO)_8]^{2-}$.

some examples in the iron chemistry,[7] because usually four metal atoms prefer to adopt either tetrahedral or butterfly arrangements. Each gold atom is bound to a phosphorus atom from the bridging dppm ligand (Au(1)–P(1) = 2.278 (2) Å and Au(2)–P(2) = 2.274 (2) Å). The Au–P bonds in **2a** with the bridging dppm ligand are practically equal to the one found in $[Fe_2(CO)_8(\mu\text{-AuPPh}_3)]^-$ (2.264 (2) Å), involving a terminal triphenylphosphine.

The short Au–Au separation is comparable to the one found in gold metal (2.884 Å),[8] so that a bonding interaction should be assumed, even if each gold atom seems almost linearly coordinated to the Fe and P atoms as indicated by the Fe(1)–Au(1)–P(1) and Fe(2)–Au(2)–P(2) angles (177.39 (8) and 172.68 (9)°, respectively). One may question if these short separations are indicative of metal–metal bonds. Au–Au interactions as short as 2.70 Å have been found in several gold(I) compounds, either with bidentate ligands or with two gold atoms bonded to a common atom (where the metals are forced to be in close contact) and with the gold atoms linearly coordinated and unexpectedly close to one another.[1] These interactions are almost perpendicular to the ligand–Au–ligand axis and seem to not disturb substantially the linear coordination at gold. An orbital explanation for such weak interactions between Au(I) ions has been reported recently.[9]

The Au–Fe distances are shorter than those found in the triangular cluster $[Fe_2(CO)_8(\mu\text{-AuPPh}_3)]^-$ and in clusters with a gold atom bridging an Fe–Fe bond (in the range 2.659–2.717 Å).[4]

The coordination around each iron atom is distorted octahedral, the bonds being to four carbonyl groups, one gold atom, and the other iron atom. The distortion in the octahedral environment is evidenced by the angles with the cis-coordinated atoms, in the range 70.3 (3)–106.7 (5)° for Fe(1) and 72.9 (3)–105.2 (5)° for Fe(2), and with trans-coordinated atoms, the narrowest being 149.7 (4)° for Fe(1) and 151.5 (5)° for Fe(2). The Fe–Fe bond distance is one of the longest Fe–Fe separations reported so far. However, it should be noted that the corresponding distance in the precursor, $[Fe_2(CO)_8]^{2-}$, is 2.787 (2) Å[10] and it is well-known that the incorporation of metal fragments such as "$MPPh_3$" in mono- or dianions lengthens the preformed metal–metal bond distances. Explanations based on steric arguments have been given.[11] Other representative examples of this effect involve the following complexes: $[Mn_2(\mu\text{-AuPMe}_2\text{Ph})(\mu\text{-PPh}_2)(CO)_8]$ (Mn–Mn distance 3.066 (8) Å) and $[Mn_2(\mu\text{-PPh}_2)(CO)_8]^-$ (2.867 (2) Å);[11] $[Os_4(\mu\text{-AuPEt}_3)(\mu\text{-H})(CO)_{13}]$ (Os–Os bond bridged distance 2.929 (2) Å)[12] and $[Os_4(\mu\text{-H})(CO)_{13}]^-$ (2.829 (2) Å (average of six Os–Os bond distances));[13] $[Fe_2(CO)_6(\mu\text{-CO})(\mu\text{-PPh}_2)]^-$ (Fe–Fe distance 2.601 (1) Å)[14] and $[Fe_2(CO)_6(\mu\text{-CO})(\mu\text{-PPh}_2)(\mu\text{-CuPPh}_3)]$ (Fe–Fe distance 2.623 (2)).[15]

Electronic Structure and Bonding Capabilities of Two Forms of $[Fe_2(CO)_8]^{2-}$. The starting anionic complex, $[Fe_2(CO)_8]^{2-}$, is known to present an unbridged structure of type A in the solid state,[10] but one can expect the doubly bridged structure B to be thermally accessible, as occurs for the isoelectronic $[Co_2(CO)_8]$.[16] Bonding of $[Fe_2(CO)_8]^{2-}$ to a $AuPR_3^+$ fragment can be regarded as the coordination of a *ligand* to a Au(I) center. Hence, our

(6) For complexes containing a planar Au_4 skeleton, see: (a) Beck, J. K.; Strahle, J. *Angew. Chem., Int. Ed. Engl.* **1986**, *25*, 95. (b) Piovesana, O.; Zanazzi, P. F. *Angew. Chem., Int. Ed. Engl.* **1980**, *19*, 561. (c) Chiari, B.; Piovesana, O.; Tarantelli, T.; Zanazzi, P. F. *Inorg. Chem.* **1985**, *24*, 366. For complexes containing a planar Ag_2Au_2 framework, see: (d) Usón, R.; Laguna, A.; Laguna, M.; Usón, A.; Jones, P. G.; Erdbrugger, C. F. *Organometallics* **1987**, *6*, 1778. (e) Abu-Salah, O. M.; Knobler, C. B. *J. Organomet. Chem.* **1986**, *302*, C10.

(7) For a nearly planar, Fe_2Ni_2 skeleton, see: Sappa, E.; Manotti Lanfredi, A. M.; Predieri, G.; Tiripicchio, A.; Carty, A. J. *J. Organomet. Chem.* **1985**, *288*, 365 and references therein. For a planar Fe_2Co_2 skeleton, see: Vahrenkamp, H.; Wucherer, E. J. *Angew. Chem., Int. Ed. Engl.* **1981**, *20*, 680. For a Fe_2NiCO skeleton, see: Muller, M.; Vahrenkamp, H. *Chem. Ber.* **1983**, *116*, 2765. For a Fe_3Rh framework, see: Ohst, H. H.; Kochi, J. K. *Organometallics* **1986**, *5*, 1359.

(8) Pearson, W. D. In *Lattice Spacings and Structure of Metals and Alloys*; Pergamon Press: London, 1957.

(9) Jiang, Y.; Alvarez, S.; Hoffmann, R. *Inorg. Chem.* **1985**, *24*, 749.

(10) Chin, H. B.; Smith, M. B.; Wilson, R. D.; Bau, R. *J. Am. Chem. Soc.* **1974**, *96*, 5285.

(11) Iggo, J. A.; Mays, M. J.; Raithby, P. R.; Henrick, K. *J. Chem. Soc., Dalton Trans.* **1984**, 633.

(12) Johnson, B. F. G.; Kaner, D. A.; Lewis, J.; Raithby, P. R.; Taylor, M. J. *J. Chem. Soc., Chem. Commun.* **1982**, 314.

(13) Dawson, P. A.; Johnson, B. F. G.; Lewis, J.; Kaner, D. A.; Raithby, P. R. *J. Chem. Soc., Chem. Commun.* **1980**, 961.

(14) Ellis, J. E.; Chen, Y.-S. *Organometallics* **1989**, *8*, 1350.

(15) Ferrer, M.; Reina, R.; Rossell, O.; Seco, M.; Solans, X. *J. Chem. Soc., Dalton Trans.* **1991**, 347.

(16) Sumner, G. G.; Klug, H. P.; Alexander, L. E. *Acta Crystallogr.* **1964**, *17*, 732. Sweany, R. L.; Brown, T. L. *Inorg. Chem.* **1977**, *16*, 415.

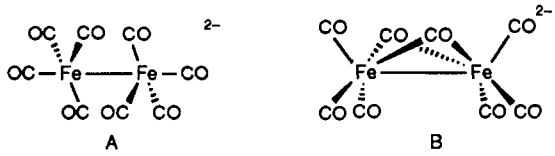

A B

theoretical study considers the bonding capabilities of the two forms of $[Fe_2(CO)_8]^{2-}$ acting as a ligand toward $AuPPh_3^+$ and tries to discover which bonding situations can be ruled out on the basis of thermodynamic grounds. The results discussed below were obtained by means of extended Hückel calculations (see Appendix for details).

We consider first the electronic structure of the unbridged form A. The metal-centered portions of the highest occupied molecular orbitals are shown in Figure 2. There are two degenerate pairs of Fe–Fe δ and δ^* orbitals, together with a σ bonding orbital. The counterintuitive ordering of the δ and δ^* orbitals is caused by the metal–ligand interactions, which predominate over the weak metal–metal δ one. Since both the δ and δ^* orbitals are occupied, four-electron repulsions result which, together with CO---CO repulsions, destabilize the eclipsed conformation in favor of the staggered one.

Notice that in A six of the carbonyl ligands are close to semibridging. In fact, the computed overlap population for the nonbonded Fe---CO interaction (0.010) suggests a weak bonding interaction and a low-energy path for its conversion to the bridged structure B. The optimized value for the Fe–Fe–C angle (α) is 82°, to be compared with the average of the experimental angles (83.3°). An orbital analysis of these interactions can be found in previous theoretical studies.[17,18] The steric hindrance of semibridging interactions in the eclipsed conformation, together with the four-electron repulsions commented on above, makes the staggered conformation somewhat more stable (the calculated barrier for rotation around the metal–metal bond is ca. 15 kcal/mol), in agreement with the structural findings.

The general aspects of the electronic structure and bonding in the bridged structure B have been discussed in detail in previous papers[17,19,20] and will not be analyzed here. However, some features of the electronic structure of the bridged form B are relevant for our study of the binding of a Lewis acid to $[Fe_2(CO)_8]^{2-}$ and deserve some attention. The molecular orbitals of $[Fe_2(CO)_8]^{2-}$ that appear in the valence region (Figure 2) have metal–metal π or π^* character and are consistent with EPR experiments on $[Fe_2(CO)_8]^-$, as shown by Krusic et al.[21] From Figure 2 it becomes evident that the highest occupied orbitals appear at higher energy than in the unbridged form A, a difference which can be traced back to the different ligand fields around the metal atoms in both structures. As a result, the unbridged structure A is calculated to be more stable (~46 kcal/mol, although no quantitative value should be ascribed to this result, given the qualitative nature of extended Hückel calculations), in agreement with the experimental structure[10] being of type A.

Let us now analyze three different ways in which the bridged and unbridged forms of $[Fe_2(CO)_8]^{2-}$ could bond to $Au(PR_3)^+$ fragments. (a) We can first rule out the possibility of forming a linear Au–Fe–Fe skeleton, since no donor orbital of $[Fe_2(CO)_8]^{2-}$ exists in that region of space, as deduced from Figure 2. (b) Equatorial attachment of the incoming acceptor can be envisaged between two equatorial carbonyls. For this job, we can use δ and δ^* combinations formed by d_{z^2}-like orbitals of Fe in the unbridged form of $[Fe_2(CO)_8]^{2-}$ (Figure 2), while no donor orbital of the right topology is available in the bridged form. (c) Finally, formation of an Fe–Au–Fe triangle requires a donor orbital localized in the region of space between both iron atoms. In structure B, electron density pops out from the metal–metal vector (a_1 orbital, Figure 2). The π orbitals in A are poorer donors because of their lower energy, their larger delocalization, and the spatial protection provided by the semibridging carbonyls. Hence, it appears that a triangular arrangement is favorable for the bridged structure of the carbonylate fragment, as appears in the structures of the $[Fe_2(CO)_8(\mu\text{-}AuPPh_3)]^-$ and $[Fe_2H(CO)_8]^-$ anions.[4]

As expected from the analysis of the molecular orbitals of $[Fe_2(CO)_8]^{2-}$ in its two forms, extended Hückel calculations indicate that $Au(PH_3)^+$ can form stable species, either in a bridging position (i.e., a triangular Fe_2Au array) with the bridged (B) form of the dianion, or in a terminal position (i.e., a rectangular or zigzag chain Fe_2Au_2 array) with its unbridged (A) form. In the bridged form, the a_1 orbital of $[Fe_2(CO)_8]^{2-}$ (Figure 2) overlaps efficiently with the empty sp_z lobe of $Au(PH_3)^+$. Some extra stabilization appears due to the π interaction between the occupied orbital b_1 and an empty p orbital of Au. The unbridged form, on the other hand, can interact with $Au(PH_3)^+$ by using a combination of its δ and δ^* orbitals in the hypothetical compound C with only one Fe–Au bond. This

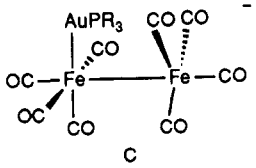

C

compound is calculated to be practically isoenergetic with the triangular compound previously reported.[4] We cannot rely on extended Hückel calculations for energetics to decide which structure is more stable for the Fe_2Au cluster, but our results suggest that both are possible and that the synthesis of the triangular isomer might be kinetically controlled. The fact that we have been able to prepare both compound **2a** with one gold attached to each iron atom and a triangular compound in which a gold is bridging both iron atoms corroborates such conclusions. Extended Hückel calculations on the model compound $[Au_2Fe_2(CO)_8(\mu\text{-}PH_2CH_2PH_2)]$ (see Appendix for details) confirm our qualitative analysis above: the d_{z^2}-like δ and δ^* orbitals of the carbonylate provide good bonding interactions with the empty lobes of both gold atoms.

It is noteworthy that there is a semibridging interaction between each gold atom and one of the cis-equatorial carbonyls (i.e., C(1) and C(7), Figure 1: Au---C distances 2.553 (9) and 2.620 (10) Å, respectively). What differentiates these two carbonyl groups from the remaining ones which are also cis to gold atoms? Our calculations on $[Au_2Fe_2(CO)_8(\mu\text{-}PH_2CH_2PH_2)]$ indicate that such interactions provide a significant contribution to the bonding of the gold and iron fragments (Au---C overlap population 0.128). Optimization of the Au–Fe–C bond angles of the *cis* carbonyls (see potential energy curves in Figure 3 and Appendix for details) reproduces the structural finding: in the most stable structure C(1) and C(7) have bond angles of ~60°, C(4) and C(6) ~80°, and C(2) and C(8)

(17) Jemmis, E. D.; Pinhas, A. R.; Hoffmann, R. *J. Am. Chem. Soc.* **1980**, *102*, 2576.
(18) Morris-Sherwood, B. J.; Powell, C. B.; Hall, M. B. *J. Am. Chem. Soc.* **1984**, *106*, 5079.
(19) Benard, M.; Dedieu, A.; Nakamura, S. *Nouv. J. Chim.* **1984**, *8*, 149.
(20) Summerville, R. H.; Hoffmann, R. *J. Am. Chem. Soc.* **1979**, *101*, 3821.
(21) Krusic, P. J.; Morton, J. R.; Preston, K. F.; Williams, A. J.; Lee, F. L. *Organometallics* **1990**, *9*, 697.

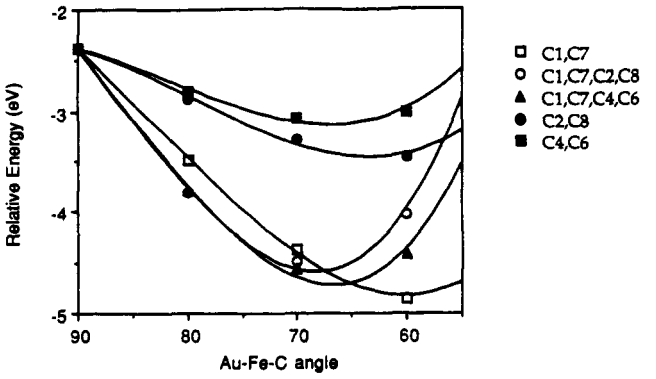

Figure 3. Total one-electron energy of $[Fe_2Au_2(CO)_8(\mu\text{-}PH_2CH_2PH_2)]$ as a function of the Au–Fe–C bond angles corresponding to the carbonyls cis to the gold atom (see Appendix for details).

~90°. Although the angle calculated for the semibridging groups is smaller than the experimental average value of 71.6°, it clearly indicates the large deviation from the expected octahedral angle of ~90°. If the carbonyls trans to the Au atoms (C(3) and C(5)) are forced into an eclipsed conformation, the minimum energy results for a symmetric structure with all four cis carbonyls at ~70°. Thus, the strong asymmetry of the cis-equatorial carbonyls is induced by the deviation of the trans groups from the eclipsed conformation (notice that the torsion angle between C(3) and C(5) is 37.9°). Schematically, the asymmetric situation around the iron atoms can be explained in the following way: (a) bonding of the $[Fe_2(CO)_8]^{2-}$ fragment to the Au_2 unit imposes an eclipsed conformation; (b) the preference of $[Fe_2(CO)_8]^{2-}$ for a staggered conformation introduces a deviation from the eclipsed one; (c) in a symmetric situation, the two cis-equatorial carbonyls set up a semibridging interaction with the gold atoms, which is favored over that of the axial carbonyls; (d) however, the deviation from the eclipsed conformation introduces an asymmetry in the potential energy surface, favoring the situation with only one semibridging equatorial interaction per gold atom.

Experimental Section

All manipulations were performed under an atmosphere of prepurified N_2 with use of standard Schlenk techniques, and all solvents were distilled from appropriate drying agents. Elemental analyses of C, H, and N were carried out at the Institut de Bio-Orgànica de Barcelona. $^{31}P\{^1H\}$ NMR spectra were obtained on a Bruker WP 80SY spectrometer. The compound $(NEt_4)_2[Fe_2(CO)_8]$ was prepared as described previously.[22] The complexes $(ClAu)_2(\mu\text{-dppm})$, $(ClAu)_2(\mu\text{-dppe})$, and $(ClAu)_2(\mu\text{-dppp})$ were synthesized and isolated as solids from ClAu(tht)[23] solutions by adding the appropriate amount of the corresponding diphosphine.

Synthesis of $[Fe_2Au_2(CO)_8(\mu\text{-dppm})]$ (2a), $[Fe_2Au_2(CO)_8(\mu\text{-dppe})]$ (2b), and $[Fe_2Au_2(CO)_8(\mu\text{-dppp})]$ (2c). Details of the synthesis of **2a** apply also to **2b,c**. To a THF (80 mL) suspension of $(NEt_4)_2[Fe_2(CO)_8]$ (0.44 g, 0.74 mmol) was added 0.62 g of $(ClAu)_2(\mu\text{-dppm})$ (0.74 mmol) at −30 °C. The mixture was warmed to 0 °C, during which time the solution became deep orange. After being stirred for an additional $^1/_2$ h, the resulting solution was filtered and precooled hexane was added to afford red air-stable microcrystals. They were collected by filtration and recrystallized from acetone–hexane yield 0.73 g (65%); IR (THF, cm^{-1}) ν(CO) stretch 2040 s, 1990 s, 1950 s, 1910 m; IR (KBr pellet, cm^{-1}) 2040 s, 1990 s, 1965 s, 1945 s, 1935 s, 1915 s, 1885 m; $\delta(^{31}P)$ = −100.0 ppm, relative to $P(OMe)_3$ (−20 °C, THF). Anal. Calcd for $[Fe_2Au_2(CO)_8(dppm)]$: C, 35.51; H, 1.97. Found: C, 35.55; H, 1.92. Spectroscopic and analytical data for the compound $[Fe_2Au_2(CO)_8(dppe)]$ (**2b**): 46% yield; IR (THF, cm^{-1}) ν(CO) stretch 2040 s, 1990 s, 1950 s, 1920 s, 1880 sh; IR (KBr pellet, cm^{-1}) 2040 s, 1990 vs, 1950 s, 1935 s, 1910 s; $\delta(^{31}P)$ = −98.1 ppm, relative to $P(OMe)_3$ (−20 °C, THF). Anal. Calcd for $[Fe_2Au_2(CO)_8(dppe)]$: C, 36.16; H, 2.12. Found: C, 36.39; H, 2.05. Spectroscopic data for the compound $[Fe_2Au_2(CO)_8(dppp)]$ (**2c**): IR (THF, cm^{-1}) ν(CO) stretch 2040 m, 1990 m, 1980 sh, 1955 sh, 1930 s, 1890 sh; $\delta(^{31}P)$ = −97.1 ppm, relative to $P(OMe)_3$ (−20 °C, THF).

Synthesis of $(NEt_4)_2[\{Fe_2Au(CO)_6(\mu\text{-}CO)_2\}_2(\mu\text{-dppe})]$ (3b) and $(NEt_4)_2[\{Fe_2Au(CO)_6(\mu\text{-}CO)_2\}_2(\mu\text{-dppp})]$ (3c). A sample of $[Fe_2Au_2(CO)_8(dppe)]$ (0.37 g, 0.33 mmol) was dissolved in 100 mL of THF at −20 °C, and 0.19 g of $(NEt_4)_2[Fe_2(CO)_8]$ (0.33 mmol) was added. The solution was stirred for 15 min and the solvent concentrated at reduced pressure to 30 mL. Slow addition of precooled hexane (20 mL) gave 0.26 g of air-unstable orange microcrystals of $(NEt_4)_2[\{Fe_2Au(CO)_6(\mu\text{-}CO)_2\}_2(\mu\text{-dppe})]$ (0.15 mmol, 46% yield): IR (THF, cm^{-1}) ν(CO) stretch 2040 w, 2000 m, 1950 s, 1910 s, 1750 m, br; IR (KBr pellet, cm^{-1}) 2040 m, 2000 s, 1955 s, 1920 s, 1895 s, 1750 m, br; $\delta(^{31}P)$ = −90.1 ppm, relative to $P(OMe)_3$ (−20 °C, THF). Anal. Calcd for $(NEt_4)_2[\{Fe_2Au(CO)_6(\mu\text{-}CO)_2\}_2(\mu\text{-dppe})]$ (**3b**): C, 40.39; H, 3.71; N, 1.62. Found: C, 39.91; H, 3.53; N, 1.50. Spectroscopic data for the compound $(NEt_4)_2[\{Fe_2Au(CO)_6(\mu\text{-}CO)_2\}_2(\mu\text{-dppp})]$ (**3c**): IR (THF, cm^{-1}) ν(CO) 2040 w, 1995 sh, 1980 sh, 1950 s, 1910 s, 1750 m, br; $\delta(^{31}P)$ = −93.2 ppm, relative to $P(OMe)_3$ (−20 °C, THF).

X-ray Data Collection, Structure Determination, and Refinement for $[Fe_2Au_2(CO)_8(\mu\text{-dppm})]$ (2a). A single crystal, ca. 0.20 × 0.23 × 0.28 mm, was selected and used for data collection. The crystallographic data are summarized in Table II. Unit cell parameters were determined from the θ values of 29 carefully centered reflections, having $11 < \theta < 19°$. Data were collected at room temperature on a Philips PW-1100 diffractometer, using graphite-monochromated Mo Kα radiation and the $\theta/2\theta$ scan type. The reflections were collected with a variable scan speed of 3–12° min^{-1} and a scan width from $(\theta - 0.65)°$ to $(\theta + 0.65 + 0.346 \tan\theta)°$. Of 6095 unique reflections, with θ in the range 3–25°, 3640 with $I \geq 2\sigma(I)$ were used for the analysis. One standard reflection was monitored every 50 measurements; no significant decay was noticed over the time of data collection. The individual profiles have been analyzed by the method of Lehmann and Larsen.[24] Intensities were corrected for Lorentz and polarization effects. A correction for absorption was applied (maximum and minimum values for the transmission factors were 1.1922 and 0.8287).[25]

The structure was solved by direct and Fourier methods and refined by full-matrix least squares, first with isotropic thermal parameters and then with anisotropic thermal parameters for all non-hydrogen atoms. All hydrogen atoms, except those at C(9) clearly localized in the final ΔF map and refined isotropically, were placed at their geometrically calculated positions (C–H = 1.00 Å) and refined "riding" on the corresponding carbon atoms. The final cycles of refinement were carried out on the basis of 432 variables; after the last cycles, no parameters shifted by more than 0.14 esd. The largest remaining peak (close to the gold atom) in the final difference map was equivalent to about 0.72 e/Å^3. In the final cycles of refinement a weighting scheme, $w = K[\sigma^2(F_o) + gF_o^2]^{-1}$, was used; at convergence the K and g values were 0.2838 and 0.0013, respectively. The analytical scattering factors, corrected for the real and imaginary parts of anomalous dispersions, were taken from ref 26. All calculations were carried out on the

Table II. Crystallographic Data for 2a

chem formula	$C_{33}H_{22}Au_2Fe_2O_8P_2$	Z	4
fw	1114.11	ρ_{calcd}, g cm^{-3}	2.145
cryst syst	monoclinic	T, °C	22
space group	$P2_1/n$	λ(Mo Kα), Å	0.710 73
a, Å	16.405 (5)	μ, cm^{-1}	94.27
b, Å	17.031 (8)	transmissn coeff	0.83–1.19
c, Å	12.410 (4)	R	0.0291
β, deg	95.64 (2)	R_w	0.0318
V, Å^3	3450 (2)		

(22) Farmery, K.; Kilner, M.; Greatrex, R.; Greenwood, N. N. *J. Chem. Soc. A* **1969**, 2339.

(23) Usón, R.; Laguna, A. *Organomet. Synth.* **1986**, *3*, 324.

(24) Lehmann, M. S.; Larsen, F. K. *Acta Crystallogr., Sect. A* **1974**, *30*, 580.

(25) Walker, N.; Stuart, D. *Acta Crystallogr., Sect. A* **1983**, *39*, 158. Ugozzoli, F. *Comput. Chem.* **1987**, *11*, 109.

Table III. Fractional Atomic Coordinates (×10⁴) and Isotropic Thermal Parameters (Å² × 10³) with Esd's in Parentheses for the Non-Hydrogen Atoms of 2a

atom	x/a	y/b	z/c	U[a]
Au(1)	3370 (1)	2551 (1)	1027 (1)	40.8 (1)
Au(2)	1648 (1)	2836 (1)	321 (1)	40.5 (1)
Fe(1)	3313 (1)	1325 (1)	-135 (1)	39.5 (4)
Fe(2)	1897 (1)	2039 (1)	-1333 (1)	41.4 (4)
P(1)	3441 (2)	3618 (1)	2138 (2)	41.7 (8)
P(2)	1558 (1)	3653 (1)	1754 (2)	38.2 (8)
O(1)	2452 (4)	983 (4)	1763 (6)	67.5 (29)
O(2)	4833 (5)	681 (5)	914 (6)	85.4 (35)
O(3)	2941 (5)	-107 (4)	-1396 (7)	88.0 (39)
O(4)	4200 (4)	2379 (4)	-1482 (6)	74.2 (34)
O(5)	2394 (5)	1203 (5)	-3219 (6)	91.5 (35)
O(6)	1015 (5)	888 (5)	-144 (7)	93.4 (40)
O(7)	2709 (4)	3546 (5)	-1597 (7)	82.4 (35)
O(8)	382 (5)	2639 (4)	-2414 (7)	84.0 (33)
C(1)	2787 (6)	1161 (5)	1019 (8)	53.6 (38)
C(2)	4223 (6)	947 (5)	514 (8)	52.4 (37)
C(3)	3080 (6)	471 (6)	-916 (8)	60.3 (41)
C(4)	3829 (5)	1981 (6)	-965 (7)	50.3 (36)
C(5)	2212 (6)	1515 (6)	-2462 (8)	61.6 (40)
C(6)	1399 (6)	1338 (6)	-583 (9)	63.2 (43)
C(7)	2398 (6)	2946 (6)	-1442 (8)	55.7 (34)
C(8)	967 (6)	2401 (6)	-1977 (8)	52.1 (37)
C(9)	2504 (5)	4231 (5)	1947 (7)	38.7 (29)
C(10)	4247 (5)	4302 (5)	1924 (8)	46.2 (34)
C(11)	4862 (6)	4082 (6)	1318 (9)	64.6 (41)
C(12)	5493 (7)	4590 (8)	1161 (11)	82.2 (57)
C(13)	5550 (7)	5303 (8)	1648 (13)	94.3 (65)
C(14)	4946 (8)	5527 (8)	2226 (14)	127.7 (81)
C(15)	4296 (7)	5042 (7)	2377 (13)	108.4 (66)
C(16)	3560 (5)	3368 (5)	3563 (7)	48.5 (34)
C(17)	3607 (8)	2623 (7)	3855 (9)	82.8 (55)
C(18)	2697 (10)	2405 (8)	4940 (11)	115.0 (75)
C(19)	3723 (8)	2950 (9)	5721 (10)	95.7 (67)
C(20)	3676 (11)	3698 (10)	5429 (11)	141.3 (85)
C(21)	3588 (10)	3917 (8)	4356 (11)	126.1 (75)
C(22)	740 (5)	4375 (5)	1660 (7)	42.6 (34)
C(23)	851 (6)	5156 (5)	1383 (8)	54.8 (39)
C(24)	186 (6)	5658 (6)	1270 (9)	67.6 (45)
C(25)	-587 (6)	5387 (7)	1404 (8)	63.9 (42)
C(26)	-691 (6)	4614 (7)	1679 (8)	61.5 (43)
C(27)	-36 (5)	4108 (6)	1790 (8)	56.0 (40)
C(28)	1462 (5)	3178 (5)	3023 (7)	40.0 (29)
C(29)	1446 (7)	2388 (5)	3092 (9)	68.4 (47)
C(30)	1378 (8)	2022 (7)	4097 (11)	99.5 (63)
C(31)	1321 (7)	2450 (7)	4997 (10)	79.0 (51)
C(32)	1322 (7)	3241 (7)	4943 (8)	74.8 (51)
C(33)	1382 (7)	3596 (6)	3957 (8)	69.1 (43)

[a] Equivalent isotropic U defined as one-third of the trace of the orthogonalized U_{ij} tensor.

Cray X-MP/48 computer of the "Centro di Calcolo Elettronico Interuniversitario dell'Italia Nord-Orientale" (CINECA, Casalecchio Bologna) and on the Gould Powernode 6040 computer of the "Centro di Studio per la Strutturistica Diffrattometrica" del CNR, Parma, Italy, using the SHELX-76 and SHELXS-86 systems of crystallographic computer programs.[27] The final atomic coordinates for the non-hydrogen atoms are given in Table III. The atomic coordinates of the hydrogen atoms are given in Table SI and the thermal parameters in Table SII.

Appendix: Computational Details

All calculations described in this paper were of the extended Hückel type[28] with modified Wolfsberg-Helmholz formula.[29] The parameters used for C, H, O, and P were the standard ones, while those for Fe[30] and Au[31] were taken from the literature. Bond distances (Å) used for the two isomers of $[Fe_2(CO)_8]^{2-}$ were as follows: Fe–C = 1.78, C–O = 1.14, Fe–Fe = 2.52, Fe–Au = 2.66, and Fe–H = 1.61. In our calculations on compound **2a** we substituted H atoms for the phenyl groups; an idealized planar structure was imposed on the $P_2Au_2Fe_2$ skeleton, and for the remaining bonding parameters we used the average of chemically equivalent distances and angles from the experimental structure. In the study of the semibridging interactions, C_2 local symmetry was imposed on the $[Fe_2(CO)_8]^{2-}$ moiety. Two-dimensional potential energy surfaces were calculated by independently changing two pairs of Au–Fe–C angles corresponding to the cis carbonyls and keeping the angle of the other pair equal to 90°, the trans carbonyls being displaced from the eclipsed situation by 38°. Several sections of such energy surfaces are presented in Figure 3. A two-dimensional surface was calculated also for the bending of the two pairs of cis equatorial carbonyls with the trans groups in the eclipsed conformation, and the minimum was found for both angles equal to ~70°.

Acknowledgment. Financial support for this work was generously given by CICYT (Spain), through grants PS87-0006 (experimental work) and PB89-0268 (theoretical studies).

Registry No. **2a**, 134132-20-0; **2b**, 134132-21-1; **2c**, 134132-22-2; **3b**, 134132-24-4; **3c**, 134132-26-6; A, 25463-33-6; $(NEt_4)_2[Fe_2(CO)_8]$, 26024-88-4; $(ClAu)_2(\mu$-dppm), 37095-27-5; $(ClAu)_2(\mu$-dppe), 18024-34-5; $(ClAu)_2(\mu$-dppp), 72428-60-5; ClAu(tht), 39929-21-0; Au, 7440-57-5; Fe, 7439-89-6; $[Fe_2Au_2(CO)_8(\mu$-$PH_2CH_2PH_2)]$, 134132-27-7.

Supplementary Material Available: Hydrogen atom coordinates (Table SI) and anisotropic thermal parameters for the non-hydrogen atoms (Table SII) (2 pages); observed and calculated structure factors (Table SIII) (21 pages). Ordering information is given on any current masthead page.

(26) *International Tables for X-Ray Crystallography*; Kynoch Press: Birmingham, England, 1974; Vol. IV.

(27) Sheldrick, G. M. SHELX-76 Program for Crystal Structure Determinations; University of Cambridge: Cambridge, England, 1976; SHELXS-86 Program for the Solution of Crystal Structures; University of Göttingen, Göttingen, Germany, 1986.

(28) Hoffmann, R. *J. Chem. Phys.* **1963**, *39*, 1397.

(29) Ammeter, J. H.; Bürgi, H.-B.; Thibeault, J. C.; Hoffmann, R. *J. Am. Chem. Soc.* **1978**, *100*, 3686.

(30) Summerville, R. H.; Hoffmann, R. *J. Am. Chem. Soc.* **1976**, *98*, 7240.

(31) Komiya, S.; Albright, T. A.; Hoffmann, R. *J. Am. Chem. Soc.* **1977**, *99*, 8440.